

Online wear detection for joints in progressing cavity pumps

J. Müller* S. Leonow* J. Schulz** C. Hansen**
M. Mönnigmann*

* *Automatic Control and Systems Theory, Ruhr-Universität Bochum, Universitätsstraße 150, 44801 Bochum, Germany (e-mail: {jens.mueller-r55, sebastian.leonow, martin.moennigmann}@rub.de).*
** *SEPEX GmbH, Scharnhölzstraße 344, 46240 Bottrop, Germany (e-mail: {jschulz, chansen}@seepe.com).*

Abstract: The wear and failure of pin joints integrated in coupling rods of process equipment can lead to unpredictable breakdown with severe consequences. We present a simple algorithm for a non-invasive online detection of wear in pin joints where a progressing cavity pump serves as an example. The algorithm only requires a pressure sensor and a binary speed signal of the motor. We verify the algorithm with a laboratory test setup and an embedded system. The results show that the proposed algorithm can reliably monitor joint wear during regular pump operation.

Keywords: fault detection, joint wear, phase-locked loop, positive displacement pumps, predictive maintenance, progressing cavity pump

1. INTRODUCTION

Progressing cavity pumps (PCPs) are very common in the process and related industries. They are essential for, e.g., applications with very viscous liquids, liquid-solid mixtures, or fluids with changing properties. Traditionally strong in the environmental and the oil and gas sector (Nelik and Brennan, 2005), today PCPs are employed over many industrial sectors from food and beverage over cosmetics to energy (see, e.g., Tan (2020)).

The classical design of a PCP features two pin joints. These joints are typically lubricated with grease or oil to limit wear. However, more than 15% of the unexpected service cases of PCPs are due to joint wear. In about 5% of the cases, the joint even breaks leading to a catastrophic pump failure. Common reasons for joint failures are damaged joint sleeves, resulting in de-lubrication of the joint due to fluid ingress. Additionally, joint failure can be caused by disregarded service intervals, extensive numbers of start-stop cycles or pump operation outside the specifications causing overload on the joints.

Joint failures cause downtimes of the entire pump and thus the process it operates in. The detection of upcoming joint failures is of major interest for pump operators. We present a novel method for predicting joint failures during run time of the pump. The proposed method is lean in that it requires only simple calculations and measurements.

We summarize the background relevant here on PCPs, their drives, and phase-locked-loops in Section 2. Section 3 presents the joint wear detection algorithm. The presentation of the laboratory test setup, the implementation of the algorithm on embedded hardware, and the experimental

results are given in Section 4. Results are summarized and discussed in Section 5.

2. PRELIMINARIES

A PCP mainly consists of two units, the rotor and the stator. During pump operation, the rotor performs an eccentric rotation inside the inner geometry of the stator. The torque provided by the electric motor must be transferred to the pump rotor either by a joint system or a flexible shaft without any slip (Wittrisch and Cholet, 2013).

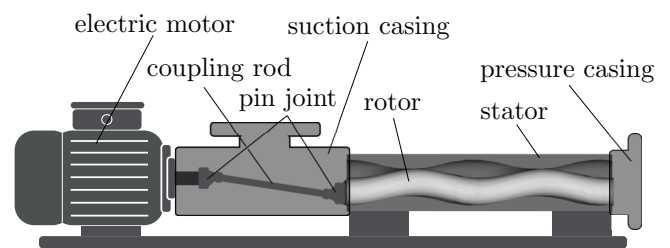


Fig. 1. Sketch of a pump unit.

We focus on single stage single lobe progressing cavity pumps with coupling rods equipped with pin joints in our contribution. Such a pump and the drive train is shown in Fig. 1. We refer to the rotational angle of the electric motor and the rotor as φ_M and φ_R , respectively. For a new pump with a coupling rod with intact joints,

$$\varphi_M = \varphi_R \quad (1)$$

holds because the coupling is torsionally rigid. We neglect any torsion of the rotating unit resulting from finite material rigidity. Furthermore, we assume that the electric motor is directly connected to the coupling rod. For pump

units with a gearbox between electric motor and coupling rod, φ_M refers to the angle on the output side of the gearbox.

2.1 Cavities and Sealings

The rotor interferes with the stator in multiple locations inside the PCP. These contact areas form a sealing pattern inside the pump and separate cavities from one another. We refer to Pan and Tan (2015) or Müller et al. (2019) for further information on the shape of the cavities and sealings.

Fig. 2 shows a sketch of the rotor-stator interaction and the cavities for several values of φ_R . Cavities progress from the suction side with pressure p_s to the pressure side with pressure p_p , conveying the fluid. A cavity open to either side attains the pressure at the respective side. Closed cavities are assumed to attain p_s (Müller et al., 2019).

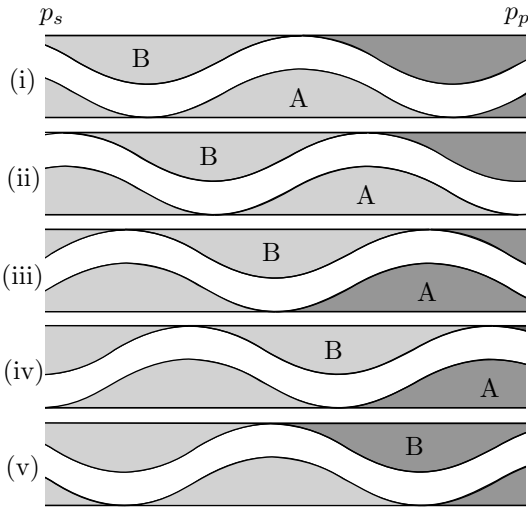


Fig. 2. Schematic cavities and according pressure distribution inside the PCP. Rotor (white) moves in the stator (solid horizontal lines) and transports cavities (e.g., those labeled A and B). Light and dark grey indicate pressure p_s and p_p , respectively.

Light and dark grey indicate p_s and p_p , respectively, in Fig. 2. As soon as a cavity with pressure p_s opens to the pressure side, the pressure inside the cavity changes abruptly. This leads to an instantaneous pressure increase inside the open cavity and an instantaneous decrease in p_p . This occurs in cavity A from step (ii) to (iii) and in cavity B from step (iv) to (v) in Fig. 2. Thus, the pressure side pressure p_p varies periodically (Belcher, 1991) as a function of the rotational angle φ_R . The periodical variation of p_p and φ_R is shown in Fig. 3 for 200 rpm and approximately 4 bar pressure side pressure. Two cavities open per rotation, thus the pressure drop of p_p occurs twice per rotor rotation.

In Fig. 3, $\varphi_R = 0$ coincides with one of the minima of p_p . This is not necessarily the case in general. In fact, the phase of the pressure pulsation is unknown after the pump assembly because it depends on the installation orientation of the stator. For an assembled pump the stator orientation and thus the phase of the pressure pulsation is unknown

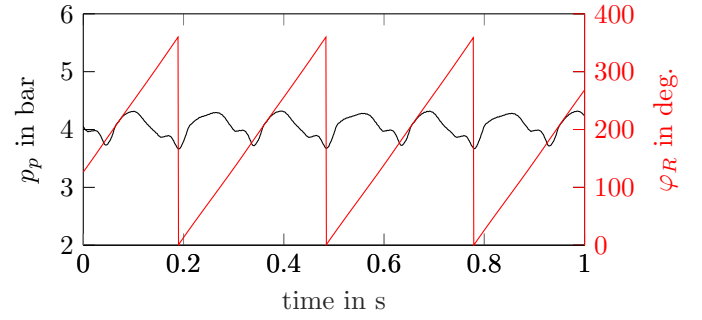


Fig. 3. Variation of p_p with respect to φ_R .

but constant. We refer to this uncertainty as the *stator phase offset* γ_0 and anticipate that it has to be taken into account for the joint wear detection in Section 2.2.

2.2 Pin joints

We treat the pin joint near the rotor (see Fig. 1) in the sequel. All results are valid for both pin joints.

Fig. 4 shows a sketch of a pin joint. The joint consists of three parts: The outer geometry (the rotor here), the inner geometry (the coupling rod here), and the pin, connecting inner and outer geometry in a torsionally rigid fashion.

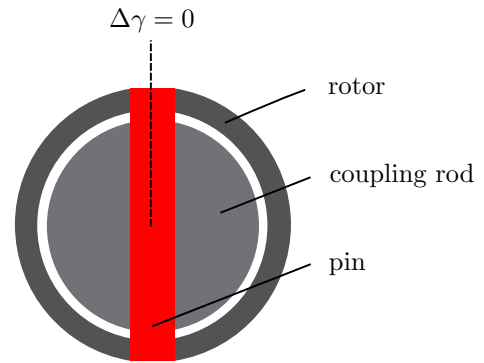


Fig. 4. Schematic pin joint in unworn condition.

The inner geometry drives the outer geometry for the joint on the rotor side. We assume that the joint rotates counter-clockwise during pump operation. The pin is held in place inside the holes of inner and outer geometry by a metallic sleeve, which is neglected in Fig. 4.

The angle $\Delta\gamma$ denotes the angle between inner and outer geometry, i.e., between rotor and coupling rod. We anticipate that $\Delta\gamma \neq 0$ results in a phase shift between rotor and coupling rod which can be used as a measure of joint wear (see Fig. 5). For a new joint, $\Delta\gamma = 0$ holds as shown in Fig. 4, resulting in (1).

The pin joints are located inside the suction casing of the pump (see Fig. 1) and encapsulated in a lubricant filled rubber sleeve to prevent the ingress of conveyed fluid. A damaged sleeve results in contact of fluid and joint components. The properties of the fluid and the lack of lubrication increase the joint wear over time.

A PCP operates with a fixed direction of rotation. Thus, the joint is only stressed in one direction of rotation

(counter-clockwise here), resulting in one-sided material loss of outer geometry, inner geometry, and pin. Fig. 5 shows a sketch of a worn pin joint.

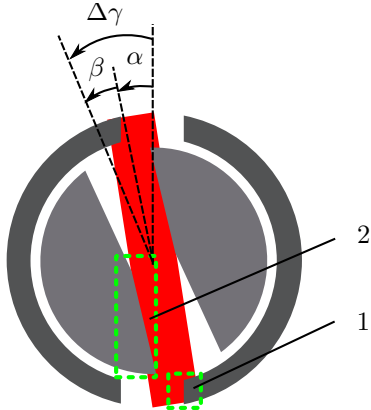


Fig. 5. Schematic pin joint in worn condition.

Two wear regions (indicated by green dashed boxes in Fig. 5) must be distinguished from one another, the wear between outer geometry and pin (region 1) and the wear between inner geometry and pin (region 2). The wear in region 1 results in a tilt of the pin (α in Fig. 5). The wear in region 2 yields the rotation of the inner geometry with respect to the pin (β in Fig. 5). Note that for both regions, wear occurs at both contacting components. According to Fig. 5, the overall phase shift between inner and outer geometry due to wear can be described by

$$\Delta\gamma = \alpha + \beta. \quad (2)$$

The coupling rod, containing the pin joints, connects the electric motor to the pump rotor (see Fig. 1). Thus, the phase shift between φ_M and φ_R depends on the joint wear $\Delta\gamma$. Additionally, the constant stator phase offset γ_0 (see Section 2.1) must be taken into account. Hence, (1) no longer applies and has to be replaced by

$$\gamma = \Delta\gamma + \gamma_0 = \varphi_M - \varphi_R, \quad (3)$$

for a pump with a worn joint. We anticipate that p_p will be used to estimate φ_R in Section 2.3. We limit the domain of γ to

$$\gamma \in [0, 180) \quad (4)$$

because p_p oscillates with twice the frequency of the rotor (see Fig. 3). We use $\Delta\gamma$ as a measure of wear and monitor $\Delta\gamma$ online.

Figure 6 (a) and (b) show a real worn pin and the driving side of the coupling rod, respectively. The green rectangle in Fig. 6 (a) indicates the initial position of the unworn pin. The components in Fig. 6 correspond to the pin and the inner geometry presented in Fig. 5. A rough analysis of the geometries shown in Fig. 6 reveals that the joint presented here reached $\Delta\gamma \approx 40^\circ$ without breaking, leading to joint failure and pump downtime.

We use the conservative threshold $\Delta\gamma_t = 30^\circ$ to distinguish acceptable from dangerously worn pin joints in the remainder of the paper. An appropriate value of $\Delta\gamma_t$ must be provided by the pump manufacturer.

Note that Fig. 6 (b) reveals that there exists wear of the coupling rod in longitudinal direction in addition to the

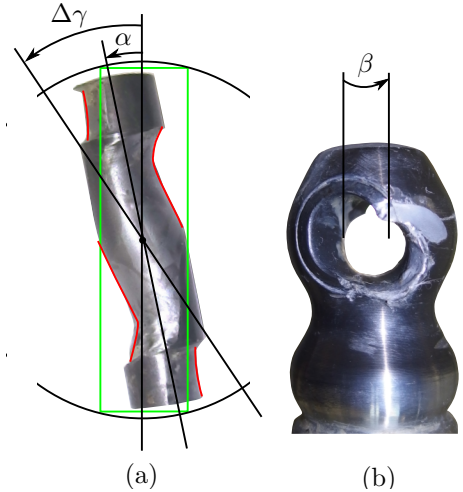


Fig. 6. Pin and coupling rod of a worn pin joint.

wear in the direction of the circumference discussed so far. We state without giving details that this longitudinal wear increases $\Delta\gamma$ and thus is accounted for by the proposed method.

We will show with experimental data in Section 4 that our algorithm can reliably detect phase shifts of $\Delta\gamma \geq 30^\circ$. Hence, the algorithm can detect joint wear before joint failure.

2.3 Phase-locked loop

Phase-locked loops (PLLs) are broadly used in industrial and scientific applications (Kroupa, 2003). It is the purpose of a PLL to estimate the phase and frequency of a periodic input signal. To this end, a generated harmonic signal is compared to the input signal. A feedback loop essentially aligns the two signals and thus provides information about the phase and frequency of the input signal. We refer to, e.g., Abramovitch (2002) for details on PLLs.

Our approach uses the periodic variation of p_p explained in Section 2.1 to estimate φ_R in an online fashion as proposed by Kouhi et al. (2020). The PLL includes a bandpass filter with a bandpass frequency of twice the rotational speed of the pump. This accounts for the opening of two cavities per rotor rotation. The use of the bandpass filter yields a periodic signal suitable for the phase and frequency estimation.

Because the bandpass frequency is a function of the rotational speed, the PLL requires the pump speed in addition to the pressure signal. The simplified block diagram is shown in Fig. 7.

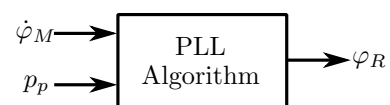


Fig. 7. Inputs and outputs of the PLL.

3. JOINT WEAR DETECTION ALGORITHM

The detection of wear inside the pin joints of the coupling rod is based on the monitoring of γ introduced in (3). Thus φ_M , φ_R , and γ_0 need to be known to determine $\Delta\gamma$.

The rotational angle φ_M can easily be measured and is available for the control of the electric motor in many industrial applications. The proposed algorithm does not require the exact measurement of φ_M at any time, but is based on the detection of a rising edge of a binary speed signal each motor rotation. This signal can easily be generated with simple and cheap retrofitted hardware, e.g., a hall sensor and a shaft-mounted magnet. We refer to the resulting peak-signal as P in the remainder of this contribution.

The motor speed $\dot{\varphi}_M$ can be calculated from P by measuring the elapsed time between two peak-signals. This calculation yields $\dot{\varphi}_M$ averaged over one rotation, which is sufficient for the proposed algorithm.

Assuming a constant pump speed, φ_M can be calculated according to

$$\varphi_M = \begin{cases} 0 & \text{if } P = 1 \\ k \cdot T \cdot \dot{\varphi}_M & \text{if } P = 0 \end{cases}, \quad (5)$$

where T is the sample time of the algorithm and k is the number of elapsed time steps after the previous occurrence of $P = 1$.

Changing the set point of the pump speed results in a transition to a new operating point. After the pump speed settled to the new stationary speed, φ_M and $\dot{\varphi}_M$ are available following one rotation of constant speed. This is sufficiently fast, as will be presented by the experimental validation in Section 4.

Due to the eccentric motion of the pump rotor (see Section 2), the axis of the rotor rotation is not constant, which complicates the direct measurement of φ_R . The hardware presented for the measurement of φ_M is thus not suitable for the measurement of φ_R . We use the PLL proposed in Section 2.3 to estimate φ_R from the variations in p_p , measured by a pressure transmitter. The pressure transmitter is not affected by the eccentric rotation and is already available in many industrial applications.

For the pump operation with unworn joints, e.g., after the assembly of a new pump, $\Delta\gamma = 0$ holds. Thus, the execution of the joint wear detection algorithm at an arbitrary point of operation yields γ_0 according to (3). Subsequently, $\Delta\gamma$ is calculated online, using γ_0 and the online estimation of γ .

When $\Delta\gamma \geq \Delta\gamma_t$ holds, joint wear is detected. We define the boolean variable S , representing the joint status, where $S = 0$ and $S = 1$ resemble unworn and worn state, respectively.

Fig. 8 shows the scheme of the joint wear detection algorithm. The eval.-block in Fig. 8 carries out the calculation of φ_M and $\dot{\varphi}_M$. The modulo function in Fig. 8 assures that (4) holds.

The joint wear can either be observed by monitoring γ and manually comparing it to γ_0 . This provides additional information about the level of wear and enables the pre-

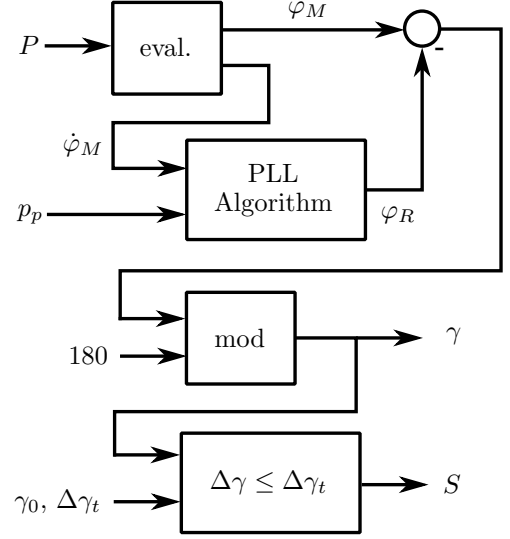


Fig. 8. Scheme of the joint wear detection algorithm.

diction of joint failure. Alternatively, the joint state S can be monitored during pump operation.

4. EXPERIMENTAL RESULTS

We validate the algorithm introduced in Section 3 with measurement data to assess the potential for an industrial application.

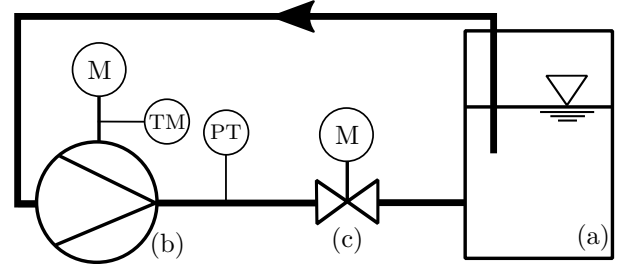


Fig. 9. Scheme of the laboratory test setup with container (a), progressing cavity pump (b), actuated valve (c), pressure transmitter (PT), Motor (M), and torque meter (TM).

4.1 Laboratory test setup

We use the laboratory test setup depicted in Fig. 9 for the validation of the joint wear detection algorithm.

The progressing cavity pump (b) pumps water from the container (a). The water passes an electrically actuated valve (c). A pressure transmitter (PT) measures the pressure side pressure p_p between the pump and the valve. The torque meter (TM) is used to generate the peak-signal P presented in Section 3. For the industrial application of the proposed algorithm a torque meter is not necessary, but a binary speed signal suffices (see Section 3).

We use the torque meter here because it was already installed in the laboratory test setup and enables the simple simulation of joint wear by adding a disturbance to

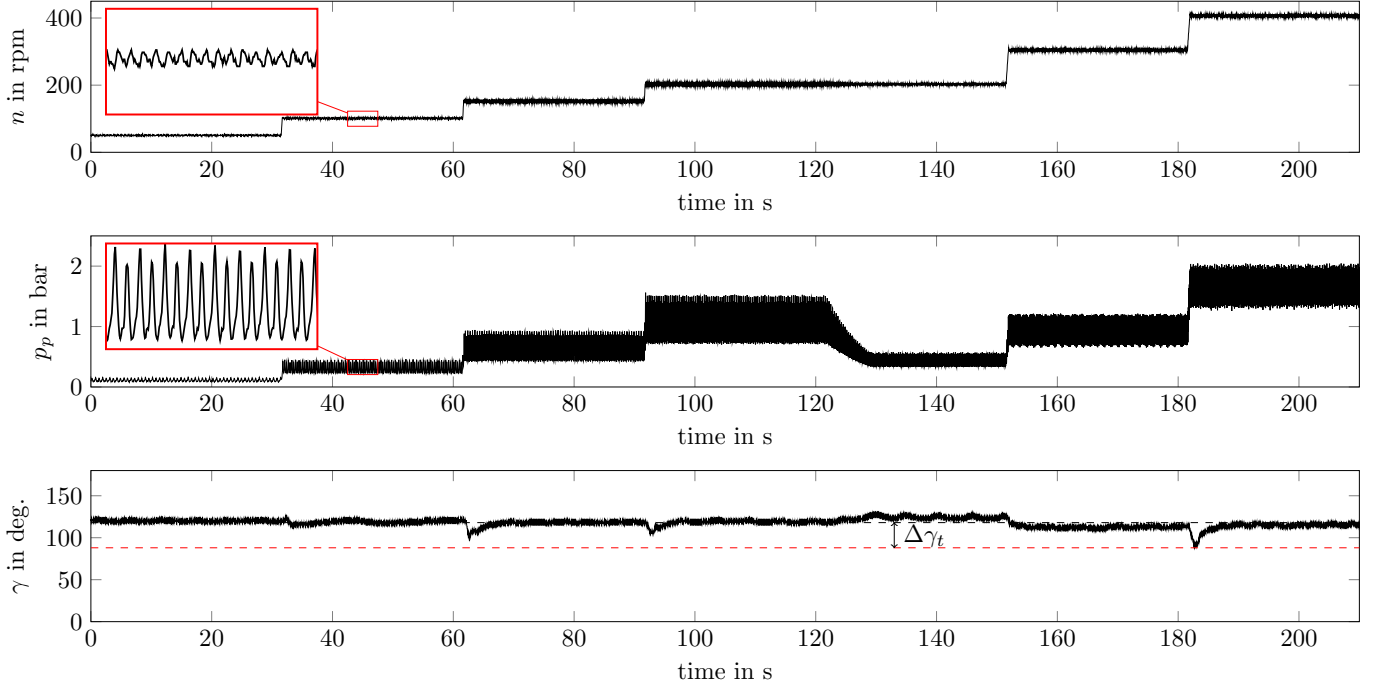


Fig. 10. Convergence of the joint wear detection algorithm for various points of operations with speeds between 50 and 400 rpm and pressures between 0.3 and 2 bar. The black and red dashed lines resemble γ_0 and γ_t , respectively.

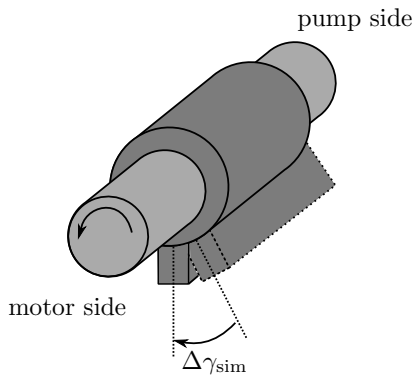


Fig. 11. Scheme of the torquemeter with the disturbance $\Delta\gamma_{\text{sim}}$.

φ_M . In general, the orientation of a torquemeter housing (dark grey in Fig. 11) is variable with respect to the measurement shaft (light grey in Fig. 11). We use this variability to simulate joint wear by manually increasing $\Delta\gamma_{\text{sim}}$ by rotating the torquemeter housing as depicted in Fig. 11.

We use $\Delta\gamma_{\text{sim}} = \Delta\gamma$ to simulate joint wear for the validation of the algorithm. The motor of the pump and the actuated valve are used to operate the pump at various speeds (n) and pressures (p_p) to simulate real pump operation.

4.2 Embedded implementation

To demonstrate the simplicity of the joint wear detection algorithm, we implement it on an embedded system. We use an 8-bit microcontroller with a speed of 16 MHz, 256 kB Memory, 8 kB RAM, an interrupt pin for the

P -signal, and two analog in- and outputs¹. These specifications reveal that the algorithm can be run on simple and cheap hardware during the operation of the pump. Hence, the embedded hardware can easily be retrofitted to existing pumps and applications.

The algorithm is executed with a sample time of 0.01 s on the embedded system. This suffices to capture the variations of p_p even for high pump speeds.

4.3 Results without simulated joint wear

Initially, we execute the joint wear detection algorithm with $\Delta\gamma_{\text{sim}} = \Delta\gamma = 0$ for various points of operation. This resembles the operation of a new pump without joint wear and thus yields γ_0 according to (3).

We operate the pump with speeds ranging from 50 to 400 rpm and pressures between 0.3 and 2 bar to cover various operational points. The results of this run are depicted in Fig. 10.

Figure 10 shows that γ converges to a similar value for all shown points of operation. Thus, the algorithm can be executed during the regular operation of the pump, reliably yielding γ_0 (marked by the black dashed line in Fig. 10). Additionally, the results in Fig. 10 show that even small values of p_p suffice for the reliable convergence of γ . Thus, the algorithm can even be used in industrial applications where p_p is small.

The distance between black and red dashed line in Fig. 10 corresponds to $\Delta\gamma_t = 30^\circ$ as proposed in Section 2.2. The algorithm returns values well above the red dashed line for all points of operation. Thus, no joint wear is detected.

¹ We use the IS.Mduino.21+ which is based on an Arduino Mega 2560 to simplify the connection to the test bench. The Algorithm is programmed and downloaded to the Arduino Board using Matlab/Simulink.

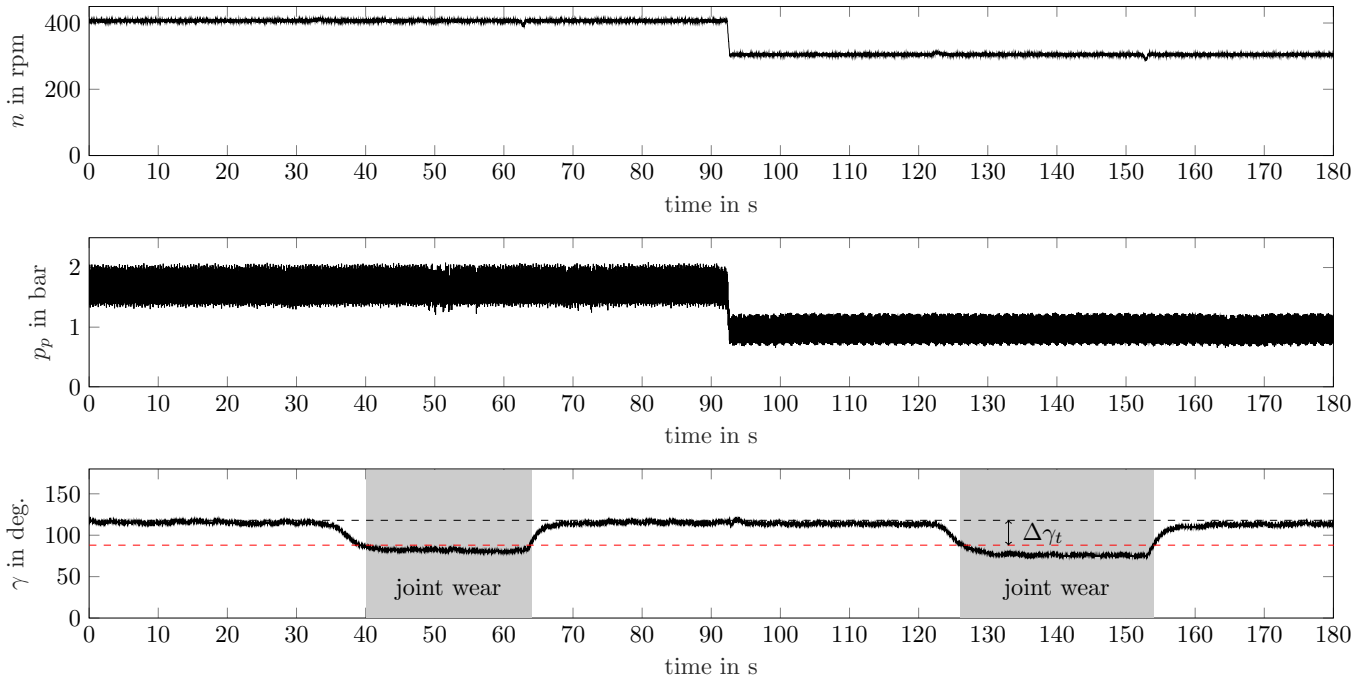


Fig. 12. Simulated joint wear by added disturbance on φ_M at 36 s and 124 s. The sections of detected joint wear ($S = 1$) are marked in gray.

The results presented in Fig. 10 were generated using only the embedded hardware.

4.4 Results with simulated joint wear

We disturb the measurement of φ_M by rotating the torquemeter by $\Delta\gamma_{\text{sim}} \approx 40^\circ$ as proposed in Section 4.1 to simulate joint wear.

The results of the joint wear detection algorithm with added disturbance are shown in Fig. 12 for two distinct points of operation. The disturbance is applied at approximately 36 s and 124 s for about 30 s each.

It is evident from Fig. 12 that the joint wear detection algorithm results in $\gamma \neq \gamma_0$ when the disturbance is applied. The sections where joint wear is detected are marked in gray in Fig. 12. These results corroborate that the proposed algorithm can be used to reliably detect joint wear during regular pump operation.

5. CONCLUSION

We presented a novel approach to detect wear of pin joints in coupling rods of process equipment without process downtime and any disassembly. The presented algorithm only relies on values provided by the manufacturer ($\Delta\gamma_t$), a reference measurement of the assembled pump without joint wear, and simple measurement signals that are already available in many industrial applications.

Furthermore, we successfully implemented the algorithm on simple and cheap hardware.

We stress that the application to a PCP serves as an example here and that the presented approach can be implemented to various types of industrial equipment with pin joints and a measurement quantity that fluctuates as a function of the rotational angle.

ACKNOWLEDGEMENTS

Funding by Ministerium für Wirtschaft, Innovation, Digitalisierung und Energie des Landes Nordrhein-Westfalen is gratefully acknowledged.

**Ministerium für Wirtschaft, Innovation,
Digitalisierung und Energie
des Landes Nordrhein-Westfalen**



REFERENCES

- Abramovitch, D. (2002). Phase-locked loops: a control centric tutorial. In *Proc. of American Control Conference (IEEE Cat. No. CH37301)*, volume 1, 1–15.
- Belcher, I. (1991). *An investigation into the operating characteristics of the progressive cavity pump*. Ph.D. thesis, Cranfield University (United Kingdom).
- Kouhi, Y., Müller, J., Leonow, S., and Mönnigmann, M. (2020). Estimating load points of a motor-pump system using pressure and inverter drive data. URL <http://arxiv.org/abs/2010.04090>.
- Kroupa, V.F. (2003). *Phase Lock Loops and Frequency Synthesis*. Wiley.
- Müller, J., Leonow, S., Schulz, J., Hansen, C., and Mönnigmann, M. (2019). Towards model-based condition monitoring for progressing cavity pumps. In *Proceedings of the 4th International Rotating Equipment Conference*, 1–10.
- Nelik, L. and Brennan, J. (2005). *Gulf Pump Guides: Progressing Cavity Pumps, Downhole Pumps and Mudmotors*. Gulf Publishing Company.
- Pan, L. and Tan, J. (2015). Numerical investigation of contact stress between rotor and stator in a two-lead progressing cavity pump. *Journal of Petroleum Science and Engineering*, 134, 176–185.
- Tan, N. (2020). *Artificial Lift Methods : Design, Practices, and Applications*. Petroleum Engineering. Springer.
- Wittrisch, C. and Cholet, H. (2013). *Progressing Cavity Pumps*. Paris, Editions Technip, second edition.